Supplementary Materials for

Rock-paper-scissors: Engineered population dynamics increase genetic stability

Michael J. Liao, M. Omar Din, Lev Tsimring, Jeff Hasty*

*Corresponding author. E-mail: hasty@ucsd.edu

Published [day] [month] 2019, *Science* **365**, 1045 (2019)
DOI: 10.1126/science.aaw0542

This PDF file includes:

Other Supplementary Material for this manuscript includes the following:
(available at science.sciencemag.org/content/365/6457/1045/suppl/DC1)

Methods

Strains and plasmids Our RPS strains were cultured in lysogeny broth (LB) media with 50μg ml-1 kanamycin and 34μg ml-1 chloramphenicol for strains containing ColE1 origin and p15A origin plasmids respectively, along with 0.2$\%$ glucose, or 50μg ml-1 spectinomycin for non-lysis colicin strains in a 37° shaking incubator. The toxins and strains used in this study are described in (**Table. S1 and S2**) and the plasmids used in this study are described in (**fig. S6**). Colicin E3 and E5 genes were assembled with overlapping PCR of gene blocks (IDT). Colicin V genes were obtained from PCR off of wild-type Colicin V *E.coli* (obtained from Dr. Joe Pogliano and Dr. Roberto Kolter). All plasmids were constructed by Gibson assembly followed by transformation into DH5α (Thermofisher) chemically competent E.coli. The primers used in this study are described in (**Table. S3**). Plasmids were verified by Sanger sequencing before transformation into E.coli strain MG1655.

Toxin co-culture To prepare colicin lysate, the appropriate colicin producing *E.coli* strains were seeded from a -80° glycerol stock into 2ml LB and incubated in a 37°C shaking incubator. After cells reached an OD600 between 0.4-0.6, 1ml of the grown culture was collected in a 2 ml eppendorf tube and two cycles of incubation at 98°C for 5 minutes followed by 10 minutes at -80°C were performed. The resulting media was then filtered and collected using a 0.22μm syringe filter.

For toxin co-culture experiments, wild type MG1655 *E.coli* strains were seeded from a -80° glycerol stock into 2ml LB and incubated in a 37°C shaking incubator. After cells reached an OD600 between 0.2-0.4, 5μl culture was added to 200μl fresh media in a standard Falcon tissue culture 96-well flat bottom plate. Additionally, 5μl of the purified colicin lysate was added to each well. Cultures were grown at 37° shaking for 19 hours and their optical density at 600nm absorbance was measured every 5 min with a Tecan Infinite M200 Pro. Fluorescence

measurements were taken every 5 min at 485 nm excitation 520 nm emission, 433 nm excitation 475 nm emission, and 590 nm excitation 630nm emission, for GFP, CFP, and RFP respectively.

Microfluidics and microscopy The microfluidic devices and experiment preparation protocols used in this study are similar to those previously reported from our group. All microfluidic experiments were performed in a side-trap array device with bacteria growth chambers approximately 100 x 80 μm in area and approximately 1.2 μm in height. The appropriate *E.coli* strain was seeded from a -80° glycerol stock into 5ml LB with the appropriate antibiotics. For lysis strain 0.2% glucose was added to the media. After growth for 8-12 h at 37° in a shaking incubator, the culture was diluted 100-fold into 25ml of the same medium in a 50ml erlenmeyer flask and grown until reaching an OD between 0.1-0.4 (Plastibrand 1.5 ml cuvettes were used). Once the above OD was reached cells were concentrated by centrifugation at 5,000g for 1 min and resuspended in 10μl of LB media with 0.075% Tween-20 and the appropriate antibiotics. This concentrate was used to vacuum-load the cells for single-strain experiments. For multi-strain experiments, cultures were first normalized to the same OD600 prior to centrifugation and mixed at either 1:1, 1:2, or 1:5 ratio for 2 strain experiments, or mixed at a 1:1:1 ratio for 3 strain experiments prior to vacuum loading. The control of media flow into the microfluidic device is gravity driven. Chip temperatures were maintained at 37°C with a plexiglass incubation chamber encompassing the entire microscope.

For sequential loading experiments the initial two strains were prepared as described for 2 strain experiments. Subsequent strains were then seeded from a -80° glycerol stock into 5ml LB with 0.2% glucose and the appropriate antibiotics. After growth for 8-12 h at 37° in a shaking incubator, the culture was diluted 100-fold into 100ml of the same medium in a 500ml erlenmeyer flask and grown until reaching an OD between 0.1-0.4 (Plastibrand 1.5 ml cuvettes were used). Once the above OD was reached cells were concentrated by centrifugation at 5,000g for 5 min and resuspended in 1ml of LB media with 0.075% Tween-20 and the appropriate

antibiotics. Cells were then loaded into a second or third inlet port of the microfluidic device, and introduced into the traps by flick loading. Flick loading was done by flicking the tygon tubing leading to the inlet of the microfluidic device, in order to disturb the laminar flow within the device to allow cells to be washed into the microfluidic traps. The control of media flow into the microfluidic device is gravity driven. For the duration of the experiment LB media containing 34μg ml-1 chloramphenicol was used. Chip temperatures were maintained at 37°C with a plexiglass incubation chamber encompassing the entire microscope.

For microscopy a Nikon Eclipse TI epifluorescent microscope with phase-contrast-based imaging was used. Image acquisition was performed with a Photometrics CoolSnap cooled CCD camera and Nikon Elements software. For 10x magnification experiments, phase-contrast images were taken with 50-100μs exposure times. Fluorescence exposure times were 100μs at 30$\%$ intensity, 300μs at 30$\%$ intensity and 100μs at 30$\%$ intensity for gfp, rfp, and cfp respectively. Images were taken either ever 3 minutes or every 6 minutes for the duration of the experiment (1-4 days). For 60x magnification experiments, phase-contrast images were taken with 20-50μs exposure times. Fluorescence exposure times were 50μs at 30$\%$ intensity, 200μs at 30$\%$ intensity and 50μs at 30$\%$ intensity for gfp, rfp, and cfp respectively. Images were taken either ever 3 minutes or every 6 minutes for the duration of the experiment (1-4 days). For sequential loading experiments, imaging was paused for the duration of strain loading.

Population Estimates and growth rate of RPS strains Population estimates for the approximate population fractions in the co-culture mixtures were made in the following way. Fluorescence channel image stacks from the dominant strain were converted to 8-bit in ImageJ (Process $>$ Binary $>$ Make Binary). Z-axis profiles were then taken for the cell incubating region (Image $>$ Stacks Plot Z-axis Profile) and the values were normalized to 1 by dividing by the max value. The max-value of the fluorescence time-series trace for the dominant strain was used as a standard for accumulated fluorescence of a culture with 100$\%$ dominant strain alone. Suscep-

tible strain fractions were estimated by subtracting the normalized dominant strain values from 1. The values were then normalized to the initial cell fractions corresponding to roughly 70% dominant strain and 30% susceptible strain. Initial cell fractions were counted manually using the ImageJ cell counter plugin.

For growth rate experiments, the appropriate *E.coli* strains were seeded from a -80° glycerol stock into 2ml LB and the appropriate antibiotics and incubated in a 37°C shaking incubator. After cells reached an OD600 of 0.1, 1ml culture was added to a 125ml erlenmeyer flask containing 25ml fresh media with appropriate antibiotics and left shaking at 270 rpm. Once the samples reached an OD600 of 0.1 samples were taken every 10 minutes and measured at OD600 using a DU 740 Life Science Uv/vis spectrophotometer.

Passage and Plate Reader Experiments For passage experiments, the appropriate *E.coli* strains were seeded from a -80° glycerol stock into 2ml LB with 0.2% glucose with the appropriate antibiotics and incubated in a 37°C shaking incubator. At an OD600 of 0.2, 10μl culture was added to 190μl fresh media containing appropriate antibiotics in a standard Falcon tissue culture 96-well flat bottom plate. Cells were incubated at 37° shaking in a Tecan Infinite M200 Pro, each passage was grown for 12 hours and the optical density at 600nm absorbance was measured every 10 min. Fluorescence measurements were taken every 10 min at 485 nm excitation 520 nm emission, 433 nm excitation 475 nm emission, and 590 nm excitation 630nm emission for GFP, CFP, and RFP respectively. After 12 hours, the OD600 of each sample was diluted to 0.2 and 10μl of each sample was passaged into 190μl of fresh media containing appropriate antibiotics in a new culture plate. For cycling strains, the appropriate *E.coli* strains were grown immediately before the appropriate passage from a -80° glycerol stock, as described before, to an OD600 of 0.2. and 10μl of the culture containing the new strain was then added to the appropriate passage before measurements were taken. Samples for Sanger sequencing were collected at the end of each passage. For analysis, a successful lysis event was defined as an

OD600 growth curve that had a defined peak followed by a drop in OD (**fig. S7**).

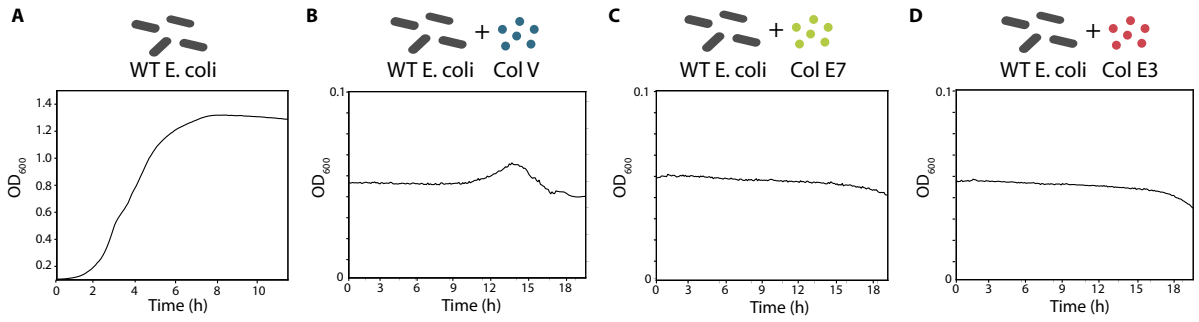

Fig. S1. Verification of Colicin activity in non-lysis strains in 96-well plate reader experiments. (**A**) Time course trace of OD600 for MG1655 wild-type *E. coli*. (**B**) Time course traces of OD600 for MG1655 wild-type *E. coli* co-incubated with filtered lysate of Colicin V producing strain. (**C**) Time course traces of OD600 for MG1655 wild-type *E. coli* co-incubated with filtered lysate of Colicin E7 producing strain. (**D**) Time course traces of OD600 for MG1655 wild-type *E. coli* co-incubated with filtered lysate of Colicin E3 producing strain.

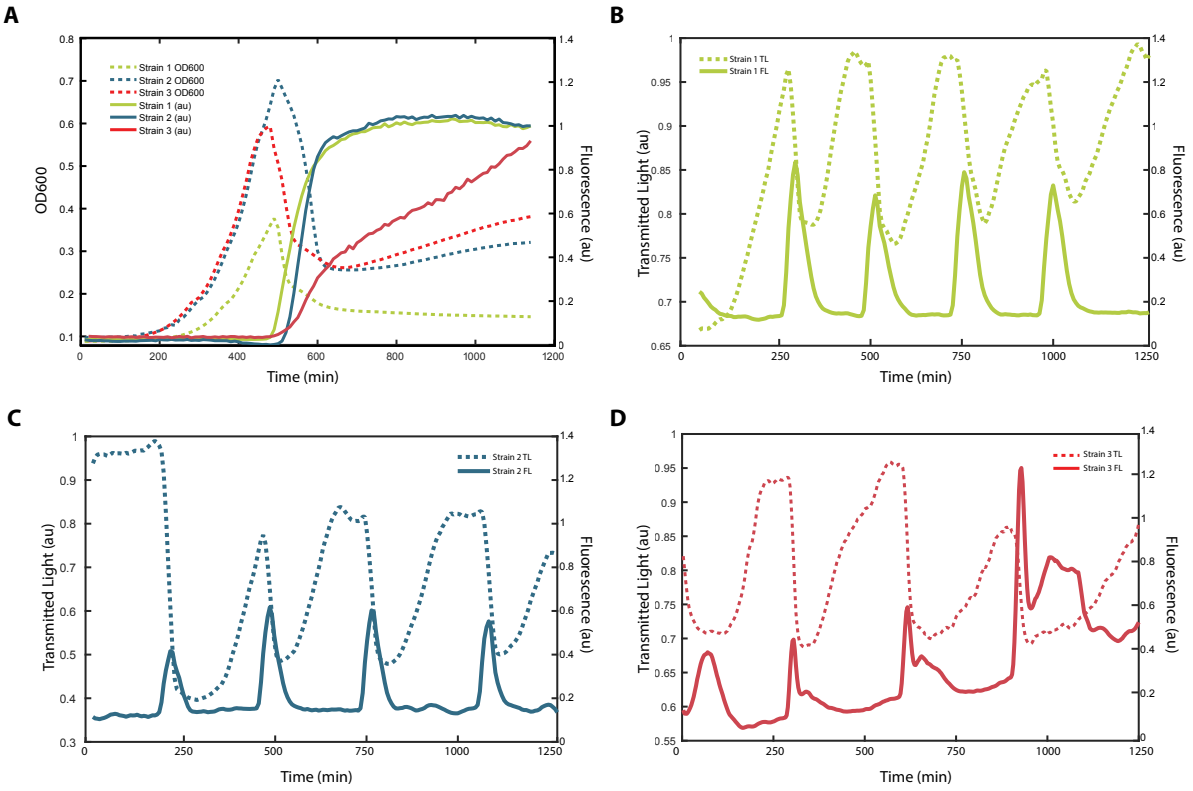

Fig. S2. Characterization of strains in both plate reader and microfluidic experiments. (**A**) Plate reader OD600 of lysis for the 3 lysis strains and the corresponding expression of fluorescence (n=3). (**B**) Overlay of Strain 1 fluorescence intensity normalized to max value (solid line) and transmitted light intensity normalized to max value (dashed line) of the microfluidic trap region (100 x 80 x 1.2 μm). (**C**) Overlay of Strain 2 fluorescence intensity normalized to max value (solid line) and transmitted light intensity normalized to max value (dashed line) of the microfluidic trap region (100 x 80 x 1.2 μm). (**D**) Overlay of Strain 3 fluorescence intensity normalized to max value (solid line) and transmitted light intensity normalized to max value (dashed line) of the microfluidic trap region (100 x 80 x 1.2 μm).

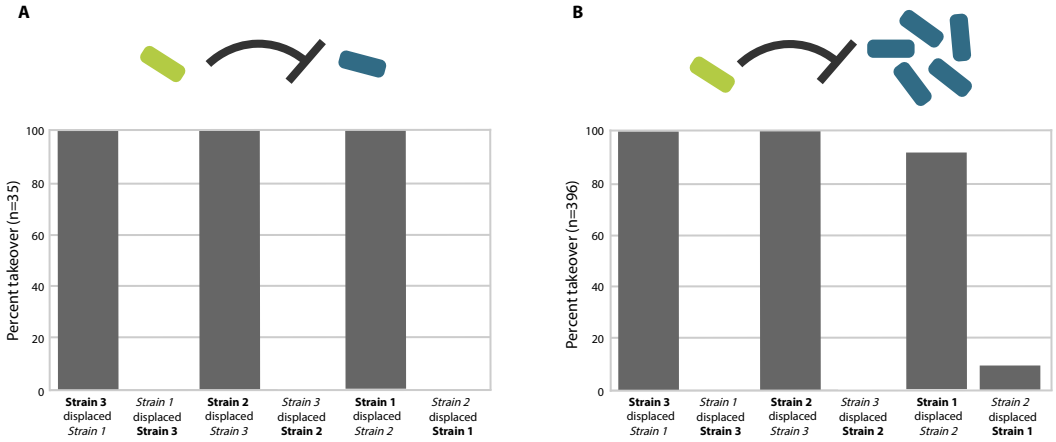

Fig. S3. Co-culture incubation of strain pairs in microfluidic devices. (**A**) Each pair of strains was co-cultured at a 1:1 ratio dominant (**bold**) to susceptible (*italic*) (n=35). For each strain pair the dominant strain displaced the susceptible strain in 100% of culture regions. (**B**) Each pair of strains was co-cultured at a 1:5 ratio dominant (bold) to susceptible (italic) (n=396). For each strain pair the dominant strain displaced the susceptible strain in 100%, 100%, and 92% of culture regions.

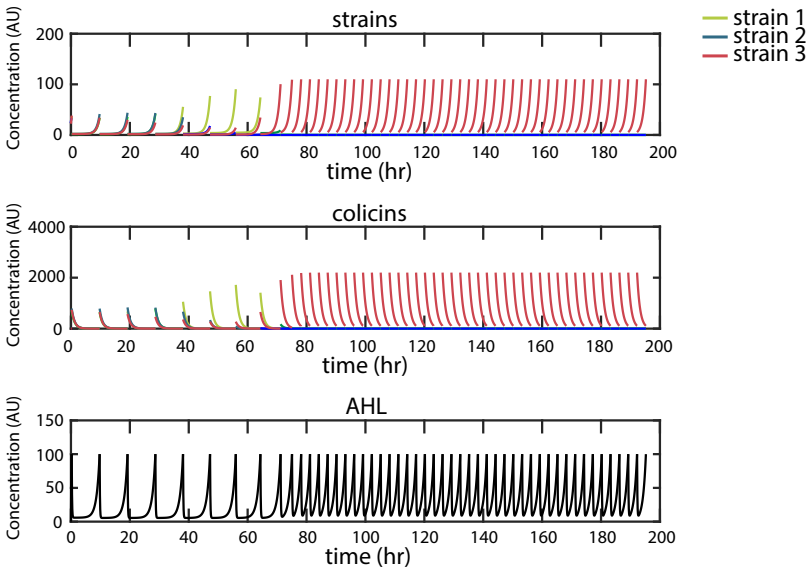

Fig. S4. Time series dynamics of the colicin model assuming the system is closed to the introduction of new cells. The three graphs show the concentrations of the strains, colicins, and AHL over time when strain 3 initially starts at a higher concentration and there is no introduction of new cells.

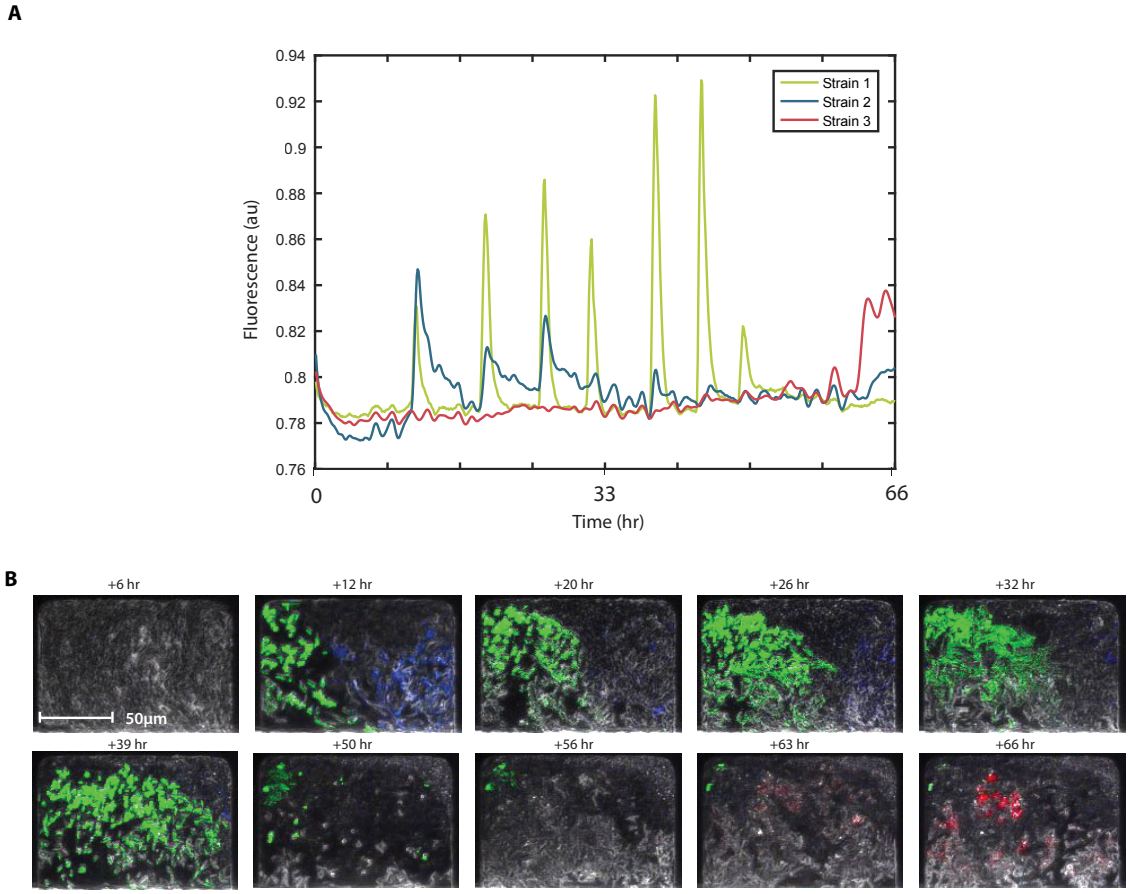

Fig. S5. Three-strain co-culture dynamics. (**A**) Time trace of GFP, CFP, and RFP fluorescence expression of a single trap from a 3-strain co-culture experiment in which all three strains are loaded at roughly equal ratios. (**B**) Video stills of phase contrast, GFP, CFP, and RFP for the microfluidic chamber shown in (**A**).

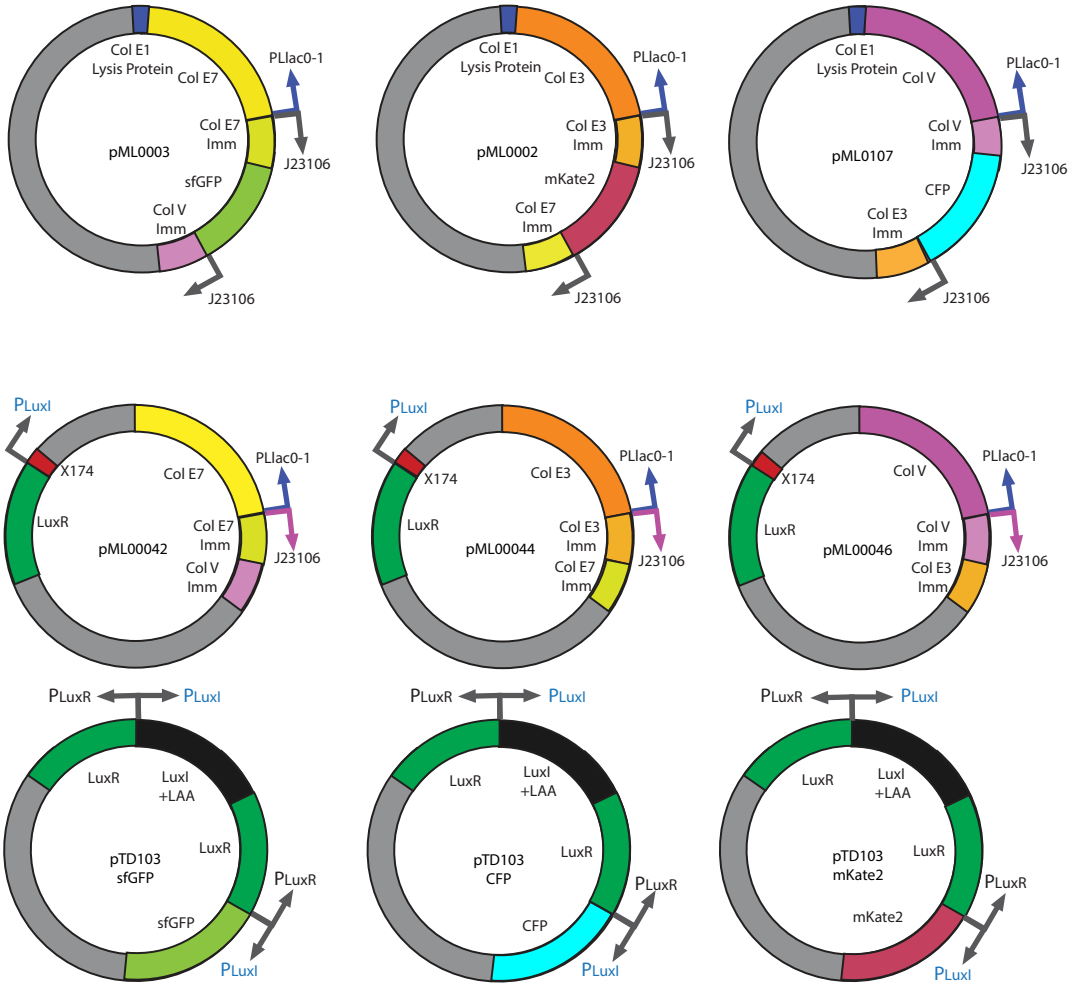

Fig. S6. The main plasmids used in this study.

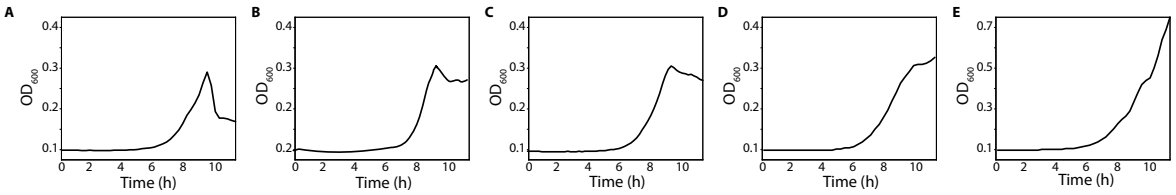

Fig. S7. Growth curve examples for succesful lysis and loss of functioning lysis. (**A**) Representative plate reader OD600 of a fresh RPS lysis strain classified as functioning lysis. (**B**) Representative plate reader OD600 of a passaged RPS lysis strain classified as functioning lysis. (**C**) Representative plate reader OD600 of a passaged RPS lysis strain classified as functioning lysis. (**D**) Representative plate reader OD600 of a passaged RPS lysis strain classified as loss of functioning lysis. (**E**) Representative plate reader OD600 of a passaged RPS lysis strain classified as loss of functioning lysis.

Toxin Type	Immunity Protein	Cytotoxic Activity	OM Receptor	Translocation Proteins
Colicin E3	Col E3 Immunity (Im3)	16s rRNase	BtuB	OmpF/TolQRAB
Colicin E7	Col E3 Immunity (Im7)	DNase	BtuB	OmpF/TolQRAB
Colicin V (Cvac)	Col V Immunity (Cvi)	Disruption of membrane potential	Cir	TonB, ExbB

Table S1. The toxins used in this study.

Strain Name	Strain #	Host Bacterium	Plasmids	Referenced in Figure
MJL003	R	MG1655	pML003 – Colicin E7 + Col E7 Immunity + sfGFP + Col V Immunity + Col E1 Lysis Protein	1b-f
MJL002	P	MG1655	pML002 – Colicin E3 + Col E3 Immunity + mKate2 + Col E7 Immunity + Col E1 Lysis Protein	1b-f
MJL107	S	MG1655	pML107 – Colicin V + Col V Immunity + CFP + Col E3 Immunity + Col E1 Lysis Protein	1b-f
MJL046	1	MG1655	pML046 – Colicin V + Col V Immunity + Col E3 Immunity + X174E (+LuxR) pTD103 sfGFP luxI (+LAA)	2b-h, 3b-d, 4b, S2, S3
MJL044	2	MG1655	pML044 – Colicin E3 + Col E3 Immunity + Col E7 Immunity + X174E (+LuxR) pTD103 CFP luxI (+LAA)	2b-h, 3b-d, 4b, S2, S3
MJL042	3	MG1655	pML042 – Colicin E7 + Col E7 Immunity + Col V Immunity + X174E (+LuxR) pTD103 mKate2 luxI (+LAA)	2b-h, 3b-d, 4b, S2, S3

Table S2. The strains used in this study.

oML0001	TTTACGGCTAGCTCAGTC
oML0009	TCAGCCCTGTTTAAATCC
oML0011	CAGCAGCGAAGTCGA
oML0013	CAGATACTGCGACCTCC
oML0021	AAGCAACCGTTATTAACATTATCC
oML0023	GGTTCCGTAATCTTAAGCG
oML0026	ATTATCGTGATGGTGATTGGT
oML0027	ATGGATAGAAAAAGAACAAAATTAGAG
oML0028	TCATTTAGAGTCAGAGTTCTC
oML0029	CCAGCCAGGACAGAAA
oML0034	TCCACTGGGTTCGTG
oML0063	AACAACTTATATCGTATGGGGC
oML0066	ATGAGAACTCTGACTCTAAATGA
oML0084	CATTTCTGTCCTGGCTGG
oML0092	AGTGCTTGGATTCTCACC
oML0093	ATTGTCACCTCCTTATCAGC
oML0094	ATTGTCACCTCCTTATCACC
oML0097	ATTGTCACCTCCTTATCATTTAG
oML0098	TGATTATCGTGATGGTGATTGGTGAT
oML0109	TTGCCGCCGGGCGTT
oML0134	GTGAAGACGGCTAGGTCTA
oML0181	TAGACCTAGCCGTCTTCAC
oML0257	AAGCCAGGATTTAAACAGGG

Table S3. The primers used in this study.

Movie S1. Strain take-over between co-cultured strains in a 100 x 80 x 1.2 μm microfluidic trap. Images taken at 60x magnification. Dominant strain S (blue) and susceptible strain P (red) demonstrate strain take-over. The bactericidal mechanism is colicin V production (Disruption of membrane potential).

Movie S2. Strain take-over between co-cultured strains in a 100 x 80 x 1.2 μm microfluidic trap. Images taken at 60x magnification. Dominant strain R (green) and susceptible strain S (grey) demonstrate strain take-over. The bactericidal mechanism is colicin E7 production (DNase).

Movie S3. Strain take-over between co-cultured strains in a 100 x 80 x 1.2 μm microfluidic trap. Images taken at 60x magnification. Dominant strain P (red) and susceptible strain R (green) demonstrate strain take-over. The bactericidal mechanism is colicin E3 production (16s rRNase).

Movie S4. Synchronized lysis between co-cultured strains in a 100 x 80 x 1.2 μm microfluidic trap. Images taken at 60x magnification. Dominant strain 1 (green) and susceptible strain 2 (blue) demonstrate integration of the synchronized lysis circuit while preserving toxin mediated strain take-over.

Movie S5. Strain take-over event in 100 x 80 x 1.2 μm microfluidic traps seeded with strain 1 (green) and strain 2 (blue) initially. Images taken at 10x magnification, 6 minute interval.

Movie S6. Strain take-over event in 100 x 80 x 1.2 μm microfluidic traps seeded with strain 2 (blue) and strain 3 (red) initially. Images taken at 10x magnification, 6 minute interval.

Movie S7. Strain take-over event in 100 x 80 x 1.2 μm microfluidic traps seeded with strain 3 (red) and strain 1 (green) initially. Images taken at 10x magnification, 6 minute interval.

COLICIN OSCILLATIONS

Let us consider three bacterial strains with densities p, q, r that in the absence of colicins grow exponentially with the same nominal growth rate which we can scale out without loss of generality. These three strains produce three types of colicins. The concentrations of these colicins in extracellular media are C_p, C_q, C_r, respectively. The role of these colicins is that they slow down the growth of each other in a circular manner: C_p slows down the growth of q, so it grows with rate $(1 + C_p)^{-1}$, C_q similarly slows down r, and C_r slows down p. Furthermore, all strains produce quorum-sensing molecules AHL , and we denote the extracellular concentration of AHL A. The colicins that cells produce remain confined to the respective cells and do not affect other strains until released into the extracellular media during lysis events. The lysis of all strains occurs if $A \geq A_c$ during which most cells get lysed, but a small fraction δ survives. The AHL in extracellular space is constantly diluted with rate γ_A, while colicins are diluted with the rate γ_C.

Suppose that at time t_i right after lysis event i, the values of all 7 concentrations are $p_i, q_i, r_1, C_p^i, C_r^i, C_q^i, A_i$, respectively. Note that by assumption $A_i = A_c$ (the lysis event is short, and the concentration of AHL does not have a chance to change). The subsequent evolution of these dynamical variables is governed by the following equations:

$$\dot{p} = \frac{p}{1 + C_r} \tag{1}$$

$$\dot{q} = \frac{q}{1 + C_p} \tag{2}$$

$$\dot{r} = \frac{r}{1 + C_q} \tag{3}$$

$$\dot{C}_p = -\gamma_C C_p \tag{4}$$

$$\dot{C}_q = -\gamma_C C_q \tag{5}$$

$$\dot{C}_r = -\gamma_C C_r \tag{6}$$

$$\dot{A} = \alpha(p + q + r) - \gamma_A A \tag{7}$$

After the lysis event i, the concentrations of p, q, r are small, and the concentration of AHL initially goes down due to dilution. But as the total bacterial density $p + q + r$ grows sufficiently large, the concentration of AHL begins to grow back. When A reaches A_c again at time t_{i+1}, new lysis event occurs, At this moment, the concentrations of the three strains that were equal to $P_{i+1}, Q_{i+1}, R_{i+1}$, respectively, are instantly reduced by the fraction δ,

$$p_{i+1} = \delta P_{i+1} + \epsilon \tag{8}$$

$$q_{i+1} = \delta Q_{i+1} + \epsilon \tag{9}$$

$$r_{i+1} = \delta R_{i+1} + \epsilon \tag{10}$$

[NOTE: we added small ϵ to avoid complete elimination of either strain. Seemingly minor, but crucial, persistent switching does not seem to occur without it]. At the same time, colicins are released from the lysed cells into the extracellular space and added to the colicins that were there before:

$$C_p^{i+1} = C_p(t_{i+1}^-) + \beta(1 - \delta)P_{i+1} \tag{11}$$

$$C_q^{i+1} = C_q(t_{i+1}^-) + \beta(1 - \delta)Q_{i+1} \tag{12}$$

$$C_r^{i+1} = C_r(t_{i+1}^-) + \beta(1 - \delta)R_{i+1} \tag{13}$$

Here $P_{i+1} = p(t_{i+1}^-)$ is the density of strain p immediately before the $i + 1$-st lysis event, and similarly for Q and R. Parameter β characterizes the release rate of colicins by bacteria during lysis (assumed to be the same for all three strains).

Simulations of Eqs. (1)-(13) show robust switching dynamics of dominant stain densities in a broad range of parameter values (Figs. 1-3).

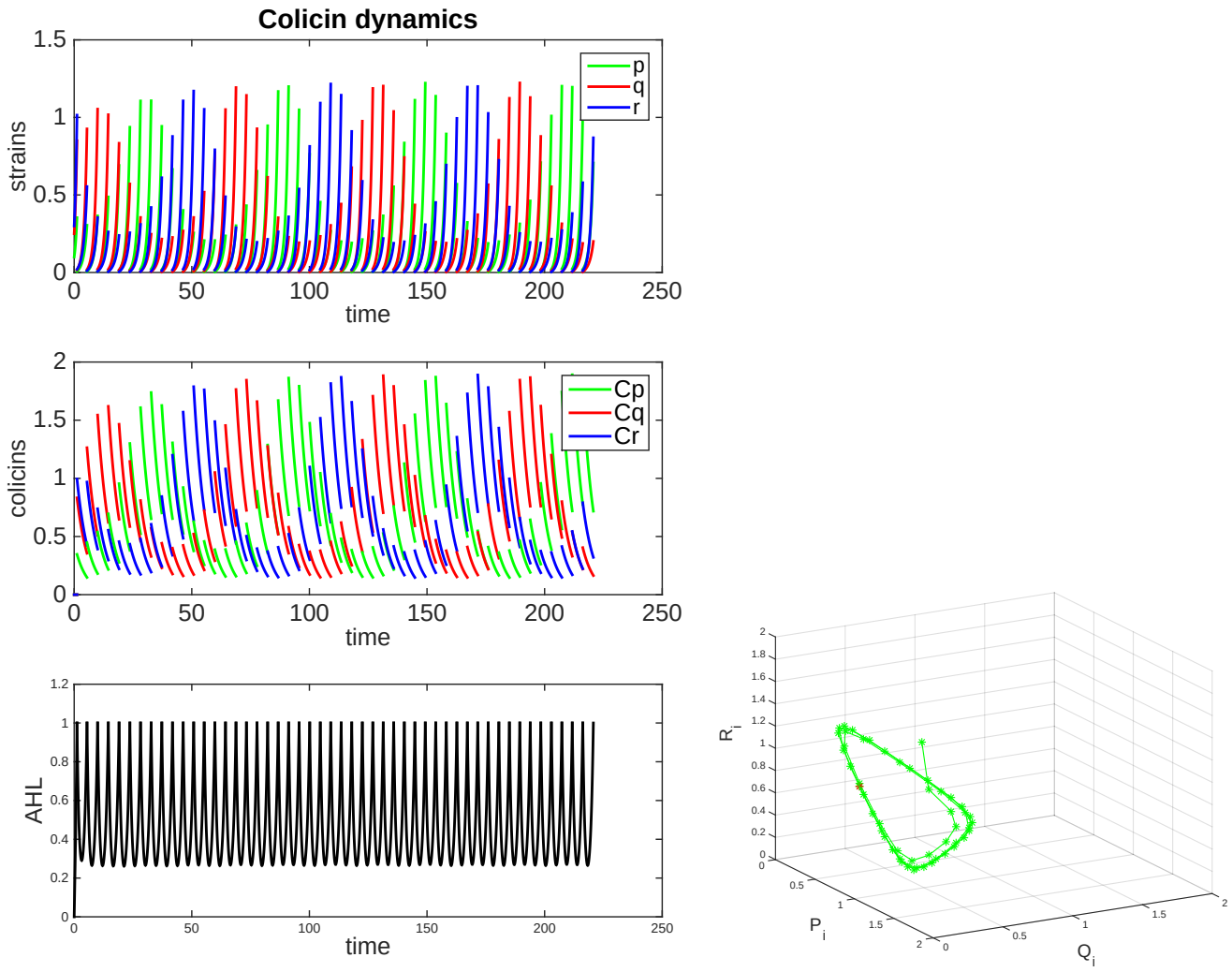

FIG. 1: Dynamics of the colicin model for $\gamma_A = 1, \gamma_C = 0.2, \alpha = 1, \beta = 1, \delta = 0.02, A_c = 1, \epsilon = 0.001$: (a) time series; (b) map of P_i, Q_i, R_i

Analytics

Equations for colicin dynamics between lysis events are linear, so they can be trivially integrated,

$$C_{p,q,r}(t) = C^i_{p,q,r} e^{-\gamma_c (t - t_i)} \tag{14}$$

Now, since we know colicin concentrations as functions of time, we can integrate equations for the strain concentrations:

$$p(t) = p_i \exp\left[\int_{t_i}^{t} \frac{dt'}{1 + C^i_r e^{-\gamma_c (t' - t_i)}}\right] = p_i \exp\left[\gamma_c^{-1} \log \frac{C^i_r + e^{\gamma_c (t - t_i)}}{C^i_r + 1}\right] = p_i \left[\frac{C^i_r + e^{\gamma_c (t - t_i)}}{C^i_r + 1}\right]^{1/\gamma_c} \tag{15}$$

$$q(t) = q_i \exp\left[\int_{t_i}^{t} \frac{dt'}{1 + C^i_p e^{-\gamma_c (t' - t_i)}}\right] = q_i \exp\left[\gamma_c^{-1} \log \frac{C^i_p + e^{\gamma_c (t - t_i)}}{C^i_p + 1}\right] = q_i \left[\frac{C^i_p + e^{\gamma_c (t - t_i)}}{C^i_p + 1}\right]^{1/\gamma_c} \tag{16}$$

$$r(t) = r_i \exp\left[\int_{t_i}^{t} \frac{dt'}{1 + C^i_q e^{-\gamma_c (t' - t_i)}}\right] = r_i \exp\left[\gamma_c^{-1} \log \frac{C^i_q + e^{\gamma_c (t - t_i)}}{C^i_q + 1}\right] = r_i \left[\frac{C^i_q + e^{\gamma_c (t - t_i)}}{C^i_q + 1}\right]^{1/\gamma_c} \tag{17}$$

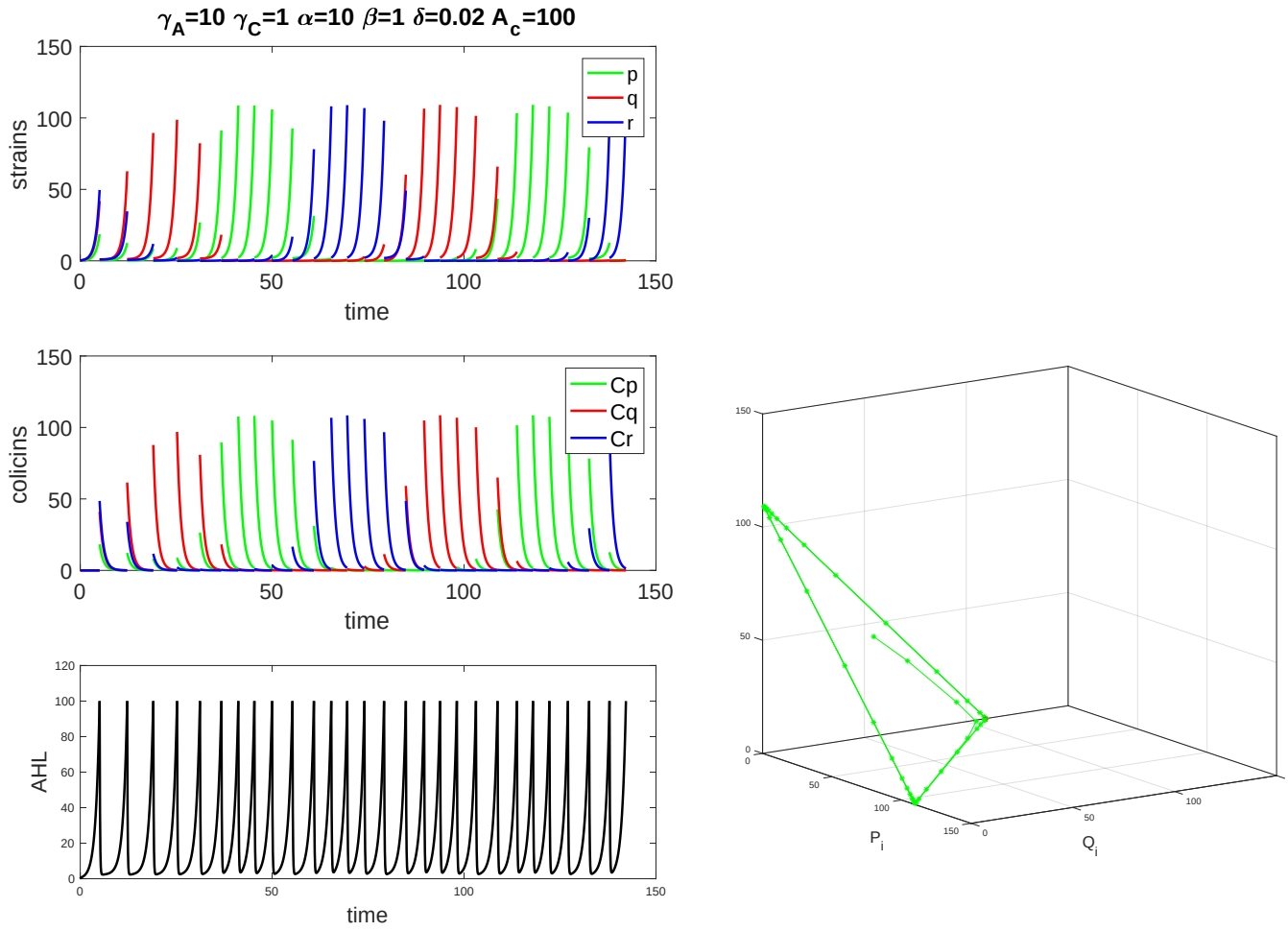

FIG. 2: Dynamics of the colicin model for $\gamma_A = 10, \gamma_C = 1, \alpha = 10, \beta = 1, \delta = 0.02, A_c = 100, \epsilon = 0.001$: (a) time series; (b) map of P_i, Q_i, R_i

Finally, we can compute the concentration of AHL between lysis events as

$$A(t) = e^{-\gamma_A(t-t_i)}\left[A(t_i) + \alpha\int_{t_i}^{t}(p+q+r)e^{\gamma_A t'}dt'\right] \tag{18}$$

The time of the next lysis event is found from the transcendental equation

$$A_c = e^{-\gamma_A(t_{i+1}-t_i)}\left[A_c + \alpha\int_{t_i}^{t_{i+1}}(p+q+r)e^{\gamma_A t'}dt'\right] \tag{19}$$

or

$$\alpha\int_{t_i}^{t_{i+1}}(p+q+r)e^{\gamma_A t'}dt' = A_c\left[e^{\gamma_A(t_{i+1}-t_i)} - 1\right] \tag{20}$$

From now own we assume that the dynamics of AHL is much faster than population dynamics (i.e. $\gamma_A \gg 1$). Then AHL concentration tracks the total amount of cells in the chamber, and the expression for A can be simplified,

$$A(t) = \alpha\gamma_A^{-1}[p(t) + q(t) + r(t)] \tag{21}$$

so the condition for the next lysis event becomes

$$P_i + Q_i + R_i = \gamma_A A_c \alpha^{-1} \tag{22}$$

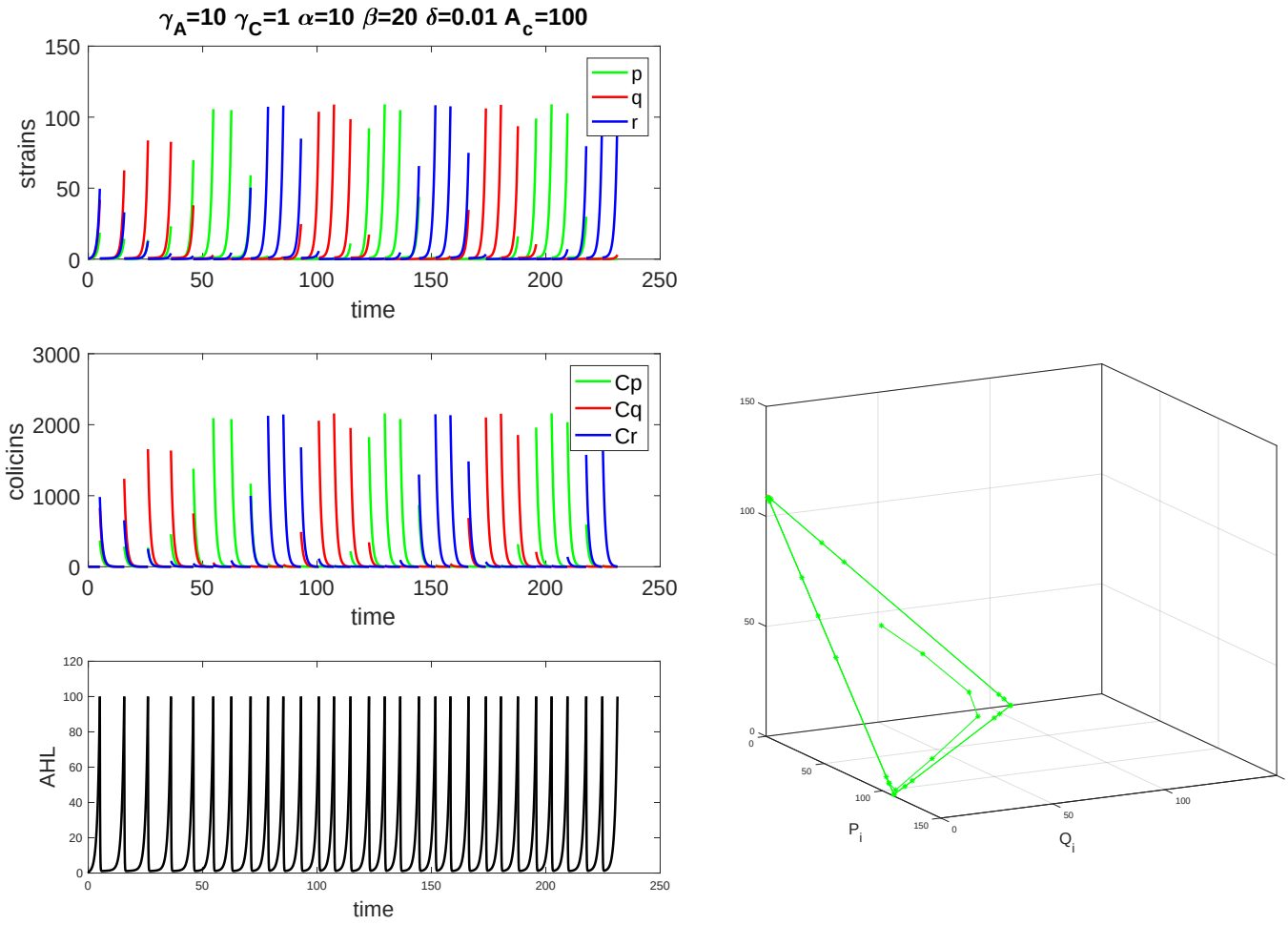

FIG. 3: Dynamics of the colicin model for $\gamma_A = 10, \gamma_C = 1, \alpha = 10, \beta = 20, \delta = 0.01, A_c = 100, \epsilon = 0.02$: (a) time series; (b) map of P_i, Q_i, R_i

If colicins also degrade sufficiently fast, so they have time to degrade to negligibly small values by the end of each lysis cycle, as in examples shown in Figs. 2, 3, then the values of C_p^i, C_q^i, C_r^i don't depend on the colicin concentrations during the previous lysis cycle, and are directly proportional to P_i, Q_i, R_i, according to Eqs. (11)-(13):

$$C_p^i = \beta(1-\delta)P_i \tag{23}$$

$$C_q^i = \beta(1-\delta)Q_i \tag{24}$$

$$C_r^i = \beta(1-\delta)R_i \tag{25}$$

Substituting these expressions and (8)-(10) in Eqs.(15)-(17) at the time of the next lysis event, $t = t_i + 1$ we get the implicit mapping

$$P_{i+1} = (\delta P_i + \epsilon)\left[1 + \frac{e^{\gamma_c T_i} - 1}{1 + \beta(1-\delta)R_i}\right]^{1/\gamma_c}, \tag{26}$$

$$Q_{i+1} = (\delta Q_i + \epsilon)\left[1 + \frac{e^{\gamma_c T_i} - 1}{1 + \beta(1-\delta)P_i}\right]^{1/\gamma_c}, \tag{27}$$

$$R_{i+1} = (\delta R_i + \epsilon)\left[1 + \frac{e^{\gamma_c T_i} - 1}{1 + \beta(1-\delta)Q_i}\right]^{1/\gamma_c}, \tag{28}$$

where we introduce the notation $T_i = t_{i+1} - t_i$ for the time interval between ith and $(i+1)$-st lysis events. The mapping is still implicit because the value T_i is still undetermined. If $\delta \ll 1$, i.e. the density of cells increases

significantly between the lysis events, one can simplify expressions in the square brackets by dropping 1's:

$$P_{i+1} = \frac{(\delta P_i + \epsilon)e^{T_i}}{(1+\beta R_i)^{1/\gamma_c}}, \tag{29}$$

$$Q_{i+1} = \frac{(\delta Q_i + \epsilon)e^{T_i}}{(1+\beta P_i)^{1/\gamma_c}}, \tag{30}$$

$$R_{i+1} = \frac{(\delta R_i + \epsilon)e^{T_i}}{(1+\beta Q_i)^{1/\gamma_c}}. \tag{31}$$

Now we can compute T_i by summing up these tree equations and using Eq. (22):

$$e^{T_i}\left[\frac{\delta P_i + \epsilon}{(1+\beta R_i)^{1/\gamma_c}} + \frac{\delta Q_i + \epsilon}{(1+\beta P_i)^{1/\gamma_c}} + \frac{\delta R_i + \epsilon}{(1+\beta Q_i)^{1/\gamma_c}}\right] = \gamma_A A_c \alpha^{-1} \tag{32}$$

In the end, we get the following explicit 3-dimensional mapping for P_i, Q_i, R_i:

$$P_{i+1} = \frac{\gamma_A A_c \alpha^{-1} X_i}{X_i + Y_i + Z_i}, \tag{33}$$

$$Q_{i+1} = \frac{\gamma_A A_c \alpha^{-1} Y_i}{X_i + Y_i + Z_i}, \tag{34}$$

$$R_{i+1} = \frac{\gamma_A A_c \alpha^{-1} Z_i}{X_i + Y_i + Z_i}, \tag{35}$$

$$\tag{36}$$

where

$$X_i = \frac{\delta P_i + \epsilon}{(1+\beta R_i)^{1/\gamma_c}}, \tag{37}$$

$$Y_i = \frac{\delta Q_i + \epsilon}{(1+\beta P_i)^{1/\gamma_c}}, \tag{38}$$

$$Z_i = \frac{\delta R_i + \epsilon}{(1+\beta Q_i)^{1/\gamma_c}}. \tag{39}$$

The interval between the lysis events, from Eq. (32), is given by

$$T_i = \log\left[\frac{\gamma_A A_c \alpha^{-1}}{X_i + Y_i + Z_i}\right]. \tag{40}$$

Fixed point and Hopf bifurcation

Let us consider the fixed point of the mapping (33)-(33) in which all three strains are equal, $P_i = Q_i = R_i = P_0 = \gamma_A A_c/3\alpha$. In this regime, the period between lysis events is given by

$$T_{fp} = \log\left[\frac{\gamma_A A_c \alpha^{-1}(1+\beta P_0)^{1/\gamma_c}}{3(\delta P_0 + \epsilon)}\right] = \log\left[\frac{\gamma_A A_c \alpha^{-1}(1+\beta\gamma_A A_c/3\alpha)^{1/\gamma_c}}{\delta\gamma_A A_c/\alpha + 3\epsilon}\right]. \tag{41}$$

To study the stability of this fixed point, we linearize the map near it,

$$\tilde{P}_{i+1} = \frac{P_0(2x_i - y_i - z_i)}{3X_0}, \tag{42}$$

$$\tilde{Q}_{i+1} = \frac{P_0(2y_i - x_i - z_i)}{3X_0}, \tag{43}$$

$$\tilde{R}_{i+1} = \frac{P_0(2z_i - x_i - y_i)}{3X_0}, \tag{44}$$

$$\tag{45}$$

where $X_0 = (\delta P_0 + \epsilon)(1+\beta P_0)^{-1/\gamma_c}$ and

$$x_i = \frac{\delta}{(1+\beta P_0)^{1/\gamma_c}}\tilde{P}_i - \frac{\beta(\delta P_0+\epsilon)}{\gamma_c(1+\beta P_0)^{1+1/\gamma_c}}\tilde{R}_i, \tag{46}$$

$$y_i = \frac{\delta}{(1+\beta P_0)^{1/\gamma_c}}\tilde{Q}_i - \frac{\beta(\delta P_0+\epsilon)}{\gamma_c(1+\beta P_0)^{1+1/\gamma_c}}\tilde{P}_i, \tag{47}$$

$$z_i = \frac{\delta}{(1+\beta P_0)^{1/\gamma_c}}\tilde{R}_i - \frac{\beta(\delta P_0+\epsilon)}{\gamma_c(1+\beta P_0)^{1+1/\gamma_c}}\tilde{Q}_i. \tag{48}$$

Substituting these expressions, we get the linear map

$$\tilde{P}_{i+1} = A(2\tilde{P}_i - \tilde{Q}_i - \tilde{R}_i) - B(2\tilde{R}_i - \tilde{P}_i - \tilde{Q}_i) \tag{49}$$

$$\tilde{Q}_{i+1} = A(2\tilde{Q}_i - \tilde{P}_i - \tilde{R}_i) - B(2\tilde{P}_i - \tilde{R}_i - \tilde{Q}_i), \tag{50}$$

$$\tilde{R}_{i+1} = A(2\tilde{R}_i - \tilde{P}_i - \tilde{Q}_i) - B(2\tilde{Q}_i - \tilde{P}_i - \tilde{R}_i), \tag{51}$$

where

$$A = \frac{\delta P_0}{3(\delta P_0+\epsilon)} = \frac{1}{3(1+3\alpha\epsilon/\delta\gamma_A A_c)}, \tag{52}$$

$$B = \frac{\beta P_0}{3\gamma_c(1+\beta P_0)} = \frac{1}{3\gamma_c(1+3\alpha/\beta\gamma_A A_c)} \tag{53}$$

The stability of the fixed point is determined by the eigenvalues of the characteristic matrix

$$\mathbf{M} = \begin{pmatrix} 2A+B & B-A & -A-2B \\ -A-2B & 2A+B & B-A \\ B-A & -A-2B & 2A+B \end{pmatrix} \tag{54}$$

This matrix has three eigenvalues: $\lambda_1 = 0, \lambda_{2,3} = 3A+3B/2 \pm i3\sqrt{3}B/2$. The first eigenvalue is zero and corresponds to super-stability. The second and third eigenvalues are complex and can correspond to exponentially growing solutions if their absolute values $|\lambda_{2,3}|$, are greater than $1, \sqrt{(3A+3B/2)^2 + 27B^2/4} > 1$, or

$$A^2 + B^2 + AB > 1/9$$

This is the condition for the Hopf bifurcation in this model. It is easy to see that for small A_c, the l.h.s. is small, but it monotonically increases with A_c to asymptotic value that is greater than 1/9, so the Hopf bifurcation always occurs at some finite A_c (see Fig. 4,a). At the Hopf bifurcation, where $|\lambda_{2,3}| = 1$, the number of lysis events per one switching cycle (1/3 of a period) is

$$N_{sw} = \frac{2\pi}{3\arcsin(3\sqrt{3}B/2)} = \frac{2\pi}{3\arcsin\left[\frac{\sqrt{3}}{2\gamma_c\left(1+\frac{3\alpha}{\beta\gamma_A A_c}\right)}\right]} \tag{55}$$

Figure 4b,c show the number of lysis pulses and bifurcation diagram for the map and the underlying full model.

Strongly switching regime

Far away from the Hopf bifurcation point, the switching becomes strongly nonlinear, when one strain dominates the dynamics for many lysis periods before rapidly switching to the next strain dmonation, and so on (Figs. 2, 3). To characterize the dynamics in this regime, we will compute the time interval between lysis events and the duration of switching cycles.

The lysis intervals vary within a switching cycle. They are smallest in the middle of the cycle, when one strain is strongly dominating, and are somewhat longer between the cycles, when two of the strains are nearly equal.

Minimum lysis interval. In the bulk of each switching cycle, one of the strains grows to high concentration at which the lysis occurs, while the other two remain much smaller (we assume that $\epsilon \ll \gamma_A A/\alpha$). In this regime, the

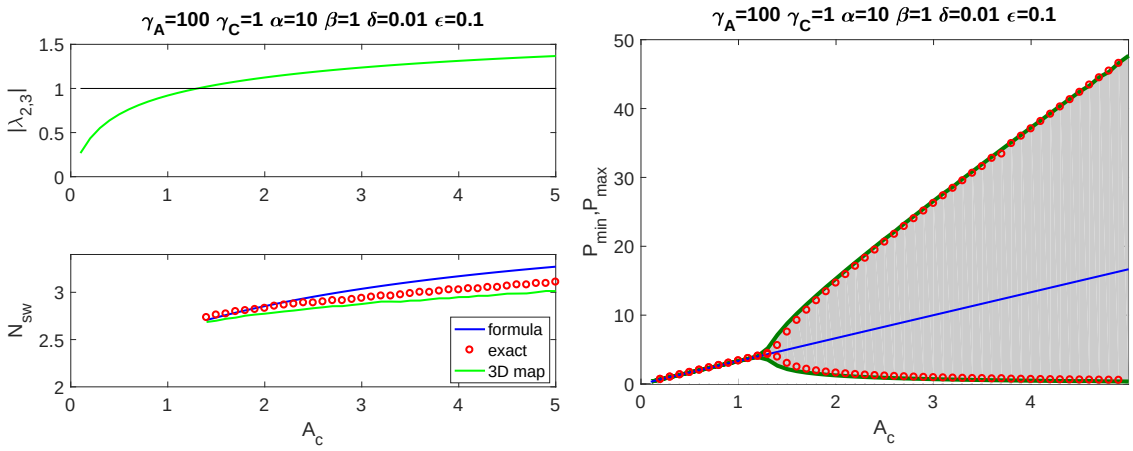

FIG. 4: (a)Magnitude of the non-zero eigenvalues of the map mode as a function of A_c. The transition to oscillations occurs at $A_c \approx 1.25$ when $|\lambda_{2,3}| = 1$. (b) Number of lysis events per switching cycle near the Hopf bifurcation. Formula (71) agrees well with the simulations at the bifurcation point, as expected. (c) Bifurcation diagram for the map model.

map becomes nearly one-dimensional and trivial (without loss of generality we choose p to be the dominating strain and assume $Q_i = R_i = 0$):

$$P_i = \gamma_A A_c \alpha^{-1} = P_M, \tag{56}$$

[we assume that $\epsilon \ll \delta\gamma_A A/\alpha$]. The interval between lysis events during this phase is

$$T_m = \log\left[\frac{P_M}{\delta P_M + 3\epsilon}\right] = -\log\left[\delta + \frac{3\epsilon\alpha}{\gamma_A A_c}\right] \approx -\log\delta. \tag{57}$$

as expected.

Maximum lysis interval. Maximum lysis interval occurs during the switch from one strain dominance to the next strain. During this switch, two of the concentrations briefly become equal at a certain $i = k+1$ (suppose, for definitiveness, $P_{k+1} = Q_{k+1}, R_{k+1} = 0$). It is easy to see that the condition of equality $P_{k+1} = Q_{k+1}$ is

$$\frac{P_k}{(1+\beta R_k)^{1/\gamma_c}} = R_k \tag{58}$$

(we neglected small ϵ here). For sufficiently sharp switch, the magnitude P_k is still close to $P_M = \gamma_A A_c/\alpha$. That allows us to solve for R_k which we can then use to find T_k. If $\beta R_k \gg 1$ (to be verified *a posteriori*) we can neglect 1 and solve this equation explicitly,

$$R_k \approx \beta^{-1}(\beta P_0)^{\frac{\gamma_c}{\gamma_c+1}} \tag{59}$$

From here, the condition of validity of this expression for $\gamma_c \sim 1$ is $\beta\gamma_A A_c \alpha \gg 1$. Now we can compute the maximum lysis interval explicitly

$$T_M = \log\left(\frac{P_M}{2\delta\beta^{-1}(P_M\beta)^{\gamma_c/(\gamma_c+1)}}\right) = -\log\delta - \log 2 - (\gamma_c+1)^{-1}\log(\beta\gamma_A A_c/\alpha). \tag{60}$$

The average lysis interval T_a is somewhere between T_m and T_M, but progressively approaches T_m as the switching intervals become longer.

Switching interval duration. To estimate the duration of the switching cycles, in which one strain dominates, we observe that it consists of two sub-intervals. In the first sub-interval, one of the strains (p , for specificity) is dominating and remains close to P_M before the lysis events, while the other two strains (q and r) are small. One of them (q) remains very small ($O(\epsilon)$) throughout the whole sub-interval since its growth is strongly suppressed by large p, while the other strain (r) is not suppressed and steadily grows from small initial level to $O(P_M)$ to eventually reach amplitudes comparable with P_M. Once this happens, the second sub-interval commences during which the amplitude

of the first strain (p) gets quickly reduced to small ($O(\epsilon)$) because its growth is now suppressed by large r. To obtain the duration of the first sub-interval, we consider the mapping for R_i, assuming that $Q_i \approx 0$, $P_i \approx P_M$

$$R_{i+1} = \delta e^{T_i}(R_i + \epsilon/\delta) \tag{61}$$

According to Eq. (32),

$$e^{T_i}\frac{\delta P_M}{(1+\beta R_i)^{1/\gamma_c}} \approx P_M \tag{62}$$

Using this expression in Eq. (31), we obtain 1D mapping

$$R_{i+1} = (R_i + \epsilon/\delta)(1+\beta R_i)^{1/\gamma_c} \tag{63}$$

To find the duration of the first sub-interval, we need to determine the number of iterations in which R_i reaches the value of the order of P_M starting from $R_0 = 0$. This sub-interval itself can be broken into two parts. While $\beta R_i \ll 1$, we can expand the second bracket and obtain the following quadratic map

$$R_{i+1} = (R_i + \epsilon/\delta)(1+\beta\gamma_c^{-1}R_i) \tag{64}$$

or introducing new variable $\hat{R}_i = \beta\gamma_c^{-1}R_i$,

$$\hat{R}_{i+1} = (\hat{R}_i + a)(1+\hat{R}_i) \tag{65}$$

with $a = \epsilon\beta/\delta\gamma_c$ and initial condition $\hat{R}_0 = 0$. For small $a \ll 1$, the number of iterations n to reach $\hat{R}_n = 1/\gamma_c$ is large and can be estimated by taking a continuous limit and integrating the following differential equation,

$$\frac{d\hat{R}}{dt} = a + a\hat{R} + \hat{R}^2 \tag{66}$$

from $\hat{R} = 0$ to $\hat{R} = 1$, which for small a yields

$$n \approx \frac{\tan^{-1}(\gamma_c^{-1}/\sqrt{a})}{\sqrt{a}} \tag{67}$$

Of course, the last few iterations the condition $\beta R_i \ll 1$ is violated, but this expression still gives a good estimation of the number of iteration needed to reach $R_n = \beta^{-1}$. Now we have to estimate the number of additional iterations for R_i to go from $R_n = \beta^{-1}$ to P_M. Since by assumption $\beta \gg \epsilon/\delta$, in this range of R_i we can neglect the latter from the map (63) and simplify it to

$$\bar{R}_{i+1} \approx \bar{R}_i(1+\bar{R}_i)^{1/\gamma_c} \tag{68}$$

where $\bar{R}_i = \beta R_i$, with initial condition $\bar{R}_n = 1$. The first several iterates of this map are as follows: $\bar{R}_{n+1} = 2^{1/\gamma_c}$, $\bar{R}_{n+2} = [2(1+2^{1/\gamma_c})]^{1/\gamma_c}$, $\bar{R}_{n+3} = [2(1+2^{1/\gamma_c})(1+[2(1+2^{1/\gamma_c})]^{1/\gamma_c})]^{1/\gamma_c}$, etc. For $\gamma_c = O(1)$, this sequence rapidly (super-exponentially) grows with i, and so already after $i = n+2$ we can neglect 1 in the brackets of Eq.(68) and write it simply as

$$\bar{R}_{i+1} \approx \bar{R}_i^{1/\gamma_c+1} \tag{69}$$

Thus, at N_1 iteration,

$$\bar{R}_{N_1} = [\bar{R}_{n+2}]^{(1+\gamma_c^{-1})^{N_c-n+2}} = [2(1+2^{1/\gamma_c})]^{\gamma_c^{-1}(1+\gamma_c^{-1})^{N_c-n-2}}$$

Equating this expression with βP_M and recalling the expression for n, we obtain the approximate formula for N_1,

$$N_1 \approx \frac{\tan^{-1}(\sqrt{\delta/\epsilon\beta\gamma_c})}{\sqrt{\epsilon\beta/\delta\gamma_c}} + \frac{\log\left[\frac{\gamma_c\log(\beta\gamma_A A_c\alpha)}{\log[2(1+2^{1/\gamma_c})]}\right]}{\log(1+\gamma_c^{-1})} + 2 \tag{70}$$

During the second sub-interval, the magnitude R_i is already near P_M, and so the growth of strain P is strongly suppressed. It means that at each lysis event it is reduced by factor δ, $P_{i+1} = \delta P_i$, This immediately yields the estimate for the number of iterations needed for P_i to reach the "background" level $O(\epsilon)$,

$$N_2 \approx \frac{\log(\epsilon P_M^{-1})}{\log \delta}$$

Thus, the total number of lysis intervals within a single switching cycle is given by

$$N_{sw} \approx \frac{\tan^{-1}(\sqrt{\delta/\epsilon\beta\gamma_c})}{\sqrt{\epsilon\beta/\delta\gamma_c}} + \frac{\log\left[\frac{\gamma_c \log(\beta\gamma_A A_c \alpha)}{\log[2(1+2^{1/\gamma_c})]}\right]}{\log(1+\gamma_c^{-1})} + 2 + \frac{\log(\epsilon P_M^{-1})}{\log \delta} \tag{71}$$

Figures 5 shows the interval between lysis events (minimal, maximal, and average) and the number of lysis events per one switching interval as functions of some model parameters, obtained from the exact model, the 3D map, and the analytical approximations. Surprisingly, the analytical approximations appear more accurate than the 3D map results.

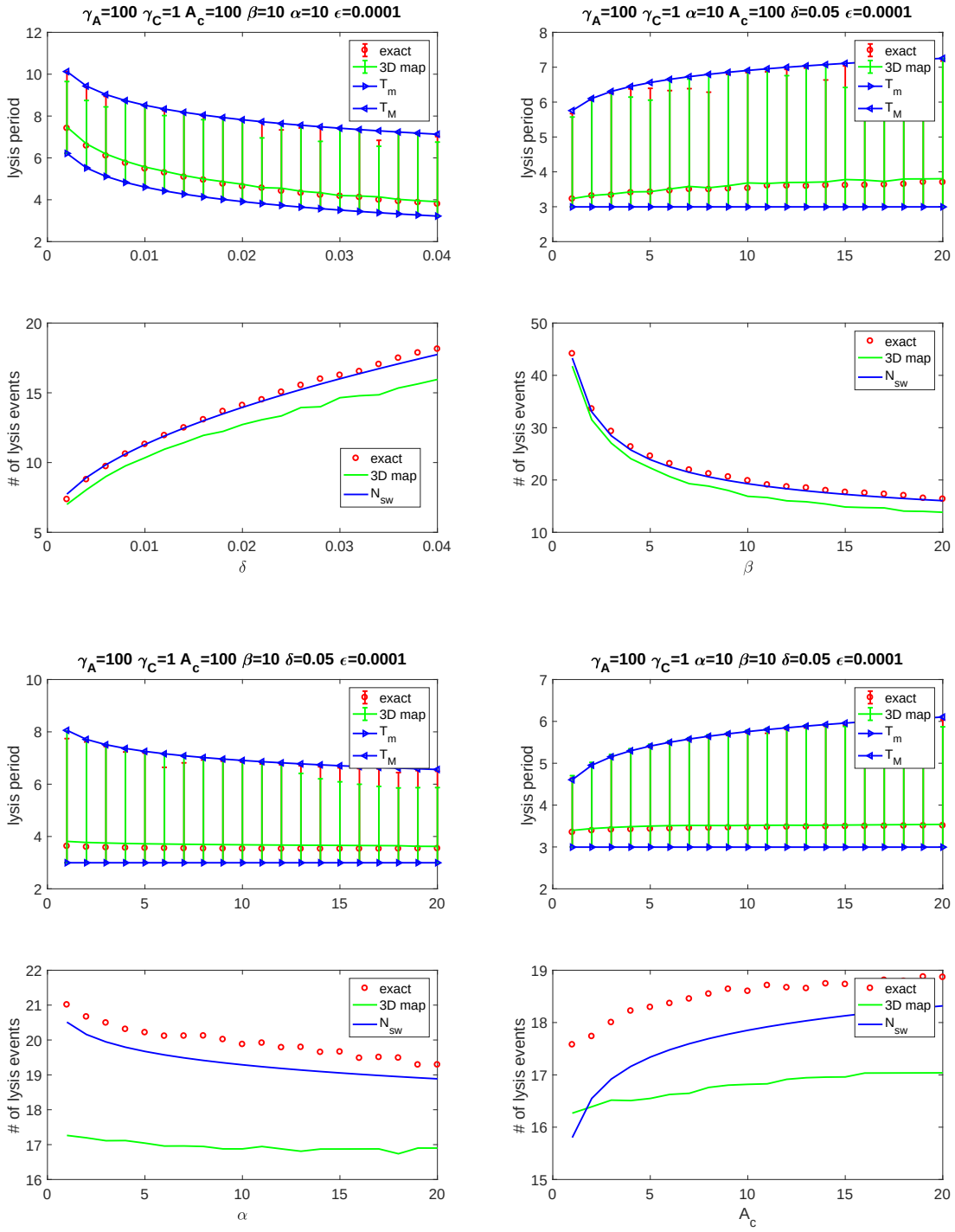

FIG. 5: Dependences of the intervals between lysis events and the number of lysis events per switching cycle on system parameters in the oscillatory regime.